Inorg. Chem. **2004**, *43*, 1943–1949

Experimental and Theoretical Investigation on the Relative Stability of the PdS_2- and Pyrite-Type Structures of $PdSe_2$

C. Soulard,[†] X. Rocquefelte,[†] P.-E. Petit,[†] M. Evain,[†] S. Jobic,*[,†] J.-P. Itié,[‡] P. Munsch,[§] H.-J. Koo, and M.-H. Whangbo*[,||]

Laboratoire de Chimie des Solides (UMR 6502), Institut des Matériaux Jean Rouxel, 2 Rue de la Houssinière, BP 32229, 44322 Nantes Cedex 3, France, Laboratoire de Physique des Matériaux Condensés (URA CNRS 782), Université Pierre et Marie Curie, 4 Place Jussieu, 75252 Paris Cedex 5, France, Laboratoire pour l'Utilisation du Rayonnement Electromagnétique (LURE), Bâtiment 209D, Centre Universitaire Paris Sud, BP 34, 91898 Orsay Cedex, France, and Department of Chemistry, North Carolina State University, Raleigh, North Carolina 27695-8204

Received October 27, 2003

Under ambient condition $PdSe_2$ has the PdS_2-type structure. The crystal structure of $PdSe_2$ under pressure (up to 30 GPa) was investigated at room temperature by X-ray diffraction in an energy-dispersive configuration using a diamond anvil cell with a mixture of water/ethanol/methanol as a pressure transmitting medium. A reversible structural transition from the PdS_2-type to the pyrite-type structure occurs around 10 GPa, and the applied pressure reduces the spacing between adjacent $^2/_\infty[PdSe_2]$ layers of the PdS_2-type structure to form the three-dimensional lattice of the pyrite-type structure. First principles and extended Hückel electronic band structure calculations were carried out to confirm the observed pressure-induced structural changes. We also examined why the isoelectronic analogues $NiSe_2$ and $PtSe_2$ adopt structures different from the PdS_2-type structure on the basis of qualitative electronic structure considerations.

1. Introduction

Structural phase transitions of transition metal dichalcogenides MQ_2 (Q = S, Se, Te) that occur under pressure are interesting because they provide rare insight into the competing forces leading to observed polymorphs. Iridium ditelluride $IrTe_2$ has the CdI_2-type layered structure under ambient condition and undergoes structural phase transitions under pressure.[1−3] An external pressure shortens the Te···Te distances and hence raises the Te 5p-block band levels thereby causing an electron transfer from the Te 5p-block to the Ir 5d-block bands. This electron transfer gives rise to a structural modification and a new charge balance between Ir and Te; the CdI_2-type structure h-$IrTe_2$, $(Ir^{3+})(Te^{1.5-})_2$, changes to a monoclinic form m-$IrTe_2$, $(Ir^{3+})_3(Te_2)^{2-}(Te^{1.75-})_4$, at 5 GPa, which in turn converts into a pyrite-type structure c-$IrTe_2$, $(Ir^{2+})(Te_2)^{2-}$, at 32 GPa. Our attempts to find similar pressure-induced transformations in CdI_2-type forms of $PdTe_2$ and $PtTe_2$ have not been successful, which is due most likely to the nearly full occupation of their d-block bands.[4] Thus, in our search for pressure-induced structural phase transitions, we shift our attention from tellurides to selenides.

Many dichalcogenides MQ_2 (Q = S, Se) of late transition metal elements M are described by the charge balance $M^{2+}(Q_2)^{2-}$. These compounds adopt the PdS_2-, the pyrite-, or the marcasite-type structure depending on how the $(Q_2)^{2-}$ dimer anions are arranged around the M^{2+} ions.[5−9] PdS_2 and $PdSe_2$ have the PdS_2-type structure, in which each square-planar Pd^{2+} (d^8) site is surrounded with four $(Q_2)^{2-}$ anions

* Authors to whom correspondence should be addressed. E-mail: jobic@cnrs-imn.fr (S.J.); Mike_Whangbo@ncsu.edu (M.-H.W.).
[†] Institut des Matériaux Jean Rouxel.
[‡] Université Pierre et Marie Curie.
[§] Centre Universitaire Paris Sud.
[||] North Carolina State University.

(1) Léger, J.-M.; Pereira, A. S.; Haines, J.; Jobic, S.; Brec, R. *J. Phys. Chem. Solids* **2000**, *61*, 27.
(2) Jobic, S.; Brec, R.; Pasturel, A.; Koo, H.-J.; Whangbo, M.-H. *J. Solid State Chem.* **2001**, *162*, 63.
(3) Jobic, S.; Brec, R.; Chateau, C., Haines, J.; Léger, J.-M.; Koo, H.-J.; Whangbo, M.-H. *Inorg. Chem.* **2000**, *39*, 4370.
(4) Soulard, C.; Jobic, S.; Whangbo, M.-H. To be published.
(5) Jobic, S.; Brec, R.; Rouxel, J. *J. Alloys Compd.* **1992**, *178*, 253.
(6) Hulliger, F. *Structural chemistry of layer type phases*; Lévy, F., Ed.; Reidel: Dordrecht, The Netherlands, 1976.
(7) Rouxel, J. *Comments Inorg. Chem.* **1993**, *14*, 207.
(8) Folmer, J. C. W.; Jellinek, J. *J. Solid State Chem.* **1988**, *72*, 137.
(9) Van Brugger, J. C. F. *Ann. Chim. (Paris)* **1982**, *7*, 171.

10.1021/ic0352396 CCC: $27.50
Published on Web 02/27/2004

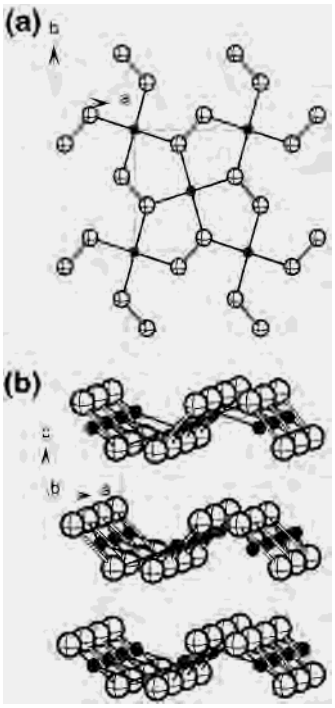

Figure 1. (a) Projection view of an isolated, puckered $PdSe_2$ layer along the direction perpendicular to the layer. (b) Perspective view of the crystal structure of $PdSe_2$. The dark circles represent the Pd atoms, and the open crossed circles represent the Se atoms. Some interatomic distances at ambient conditions are the following: intralayer Pd−Se = 2.4412(2) Å, intralayer Se−Se = 2.3783(3) Å, interlayer Pd···Se = 3.2610(2) Å, and interlayer Se···Se = 3.7412(3) Å.

to form puckered PdQ_2 layers (Figure 1a), and these PdQ_2 layers are well separated from each other to have van der Waals gaps between them (Figure 1b). NiS_2 and $NiSe_2$ are isoelectronic with PdS_2 and $PdSe_2$ but adopt the pyrite-type structure in which each octahedral Ni^{2+} (d^8) site is surrounded with six $(Q_2)^{2-}$ anions forming a compact three-dimensional lattice.[5,7] In the case of platinum dichalcogenides PtQ_2, which are also isoelectronic with PdQ_2, the CdI_2-type structure is observed.[10] The PdS_2- and pyrite-type structures of MQ_2 are closely related.[6] When the puckered MQ_2 layers of the PdS_2-type structure are compressed toward each other, the two empty axial positions of each square-planar M^{2+} site become occupied by the $(Q_2)^{2-}$ anions of two adjacent MQ_2 layers and, as a result, the pyrite-type structure emerges. Thus, it is possible to convert the structure of PdQ_2 from the PdS_2- to the pyrite-type by applying pressure as already suggested by Larchev et al.[11] In the present work, we probe this implication by carrying out powder X-ray diffraction measurements of $PdSe_2$ as a function of pressure up to 30 GPa and by optimizing the crystal structure of $PdSe_2$ under pressure in terms of first principles electronic band structure calculations. In addition, we examine why PdQ_2 (Q = S, Se) adopts the PdS_2-type structure whereas NiQ_2 and PtQ_2 adopt different structures on the basis of qualitative electronic structure considerations.

(10) Dai, D.; Koo, H.-J.; Whangbo, M.-H.; Soulard, C.; Rocquefelte, X.; Jobic, S. *J. Solid State Chem.* **2003**, *173*, 114.
(11) Larchev, V. I.; Popova, S. V. *Neorg. Mater.* **1978**, *14*, 775.

2. Experimental Section

2.1. Structure of $PdSe_2$ under Ambient Pressure. A stoichiometric mixture of elemental powders (Pd sponge, 229 mg, 99.9% Aldrich; Se pellets, 340 mg, >99.995% Fluka) was ground and loaded into a quartz tube (9 cm in length, 8 mm in interior diameter). The tube was evacuated to 10^{-2} Torr, sealed, and placed into a furnace which was raised at 850 °C (rate of 5 °C/h) for 600 h, as referenced by Lieth et al.[12] The powder sample was subsequently cooled at room temperature at 5 °C/h. This procedure led to pure $PdSe_2$ powdered sample. Single crystals were easily prepared by transport reaction with iodine (I_2, resublimed crystals, TMI 10 ppm, Alfa) in tubes of 20-cm in length.

X-ray diffraction data were collected on a CPS 120 INEL diffractometer for powder samples, and on an Enraf-Nonius CAD4-*F* diffractometer for a single-crystal sample. The structure refinements were carried out using the Jana2000 software package.[13] The details of the crystallographic data are summarized in Table 1. The structural parameters are in good agreement with those reported in the literature (relative deviations not larger than 0.2%).[14]

As already mentioned, the $PdSe_2$ structure consists of $PdSe_2$ layers in which palladium atoms are located in square planar coordinate sites made up of Se_2 dimers (Figure 1a). The corrugation height, Δz, of each puckered $PdSe_2$ layer is ca. 1.43 Å, and the $PdSe_2$ layers are separated by van der Waals gaps with the shortest interlayer Se···Se distance of 3.7412 (3) Å (Figure 1b).

2.2. Diffraction Measurements under High Pressure. Sample Setting in the High-Pressure Cell. Samples were compressed in a membrane-type diamond anvil cell. Standard Drukker diamonds anvils with culets 500 μm in diameter were mounted. The rhenium gaskets used were preindented to a thickness of 40 μm and drilled to a diameter of 200 μm. $PdSe_2$ powder samples were ground to a fine powder in an agate mortar and loaded in the pressure chamber. A mixture of water/ethanol/methanol in the ratio 1:3:16 was used as a pressure-transmitting medium to provide quasihydrostatic pressure conditions.

Optical Geometry and Pressure Measurements. Ruby grains were mixed with the powder sample to measure the in-situ pressure. The fluorescence emission of the ruby was obtained using a laser beam of a 100 mW argon laser.[15] The fluorescence emission of the ruby grains was systematically measured before and after applying pressure for each run to establish the relationship between the pressure and the position of the fluorescence lines as P(GPa) $= 380.8\{[1 + (\Delta\lambda/\lambda_0)]^5 - 1\}$[16] with $\lambda_0 = 694.2$ μm.

X-ray Diffraction Measurements and Data Analysis. Our experiments were carried out in an energy-dispersive mode using a Canberra Ge solid-state detector with a resolution ranging from 145 eV at 5.9 keV to 335 eV at 59.5 keV. The latter values are close to the theoretical limit of the detector and are achieved by selecting a sample−detector distance of 200 mm and using a vertical secondary slit system. After the calibration of the energy of the detector, the 2θ angle was determined by collecting the diffraction pattern of copper. The diffraction spectra were then recorded for energies ranging from 3 to 60 keV at $2\theta = 11.170(1)°$. The electronic beam, operating at the intensity of 200 mA and the energy

(12) Lieth, R. M. A.; Terhell, C. J. M. *Preparation and crystal growth of materials with layered structures*; D. Reidel Publishing Company: Dordrecht, Holland.
(13) Petricek, V.; Dusek, M. *Jana2000. Crystallographic computing system*; Institute of Physics: Praha, Czech Republic, 2000.
(14) Gronvold, F.; Rost, E. *Acta Crystallogr.* **1957**, *10*, 329.
(15) Fiquet, G.; Andrault, D.; Itié, J.-P.; Gillet, P.; Richet, P. *Phys. Earth Planet. Inter.* **1996**, *95*, 1.
(16) Xu, J. A.; Mao, H. K.; Bell, P. M. *Science* **1986**, *232*, 1404.

Table 1. Crystal Structure of $PdSe_2$ Determined at 298 K under Ambient Pressure by Single Crystal and Powder X-ray Diffraction

(a) Crystallographic Data, X-ray Data Collection, and Refinement Parameters

Physical and Crystallographic Data	
chemical formula	$PdSe_2$
mol wt ($g \cdot mol^{-1}$)	264.30
syst	orthorhombic
space group	*Pbca* (No. 61)
cell parameters[a]	$a = 5.7457(4)$ Å
	$b = 5.8679(4)$ Å
	$c = 7.6946(3)$ Å
V	259.43(5) $Å^3$
Z	4
calcd density	6.770
abs coeff	34.996 cm^{-1}
Recording Conditions	
diffractometer	Enraf-Nonius CAD4-*F*
radiation	Mo $KL_{2,3}$ (0.71069 Å)
angular range	$2\theta = 5.31-39.96°$
hkl range	$-10 \le h \le 10$
	$-10 \le k \le 10$
	$-13 \le l \le 7$
total recorded reflns	4876
obsd reflns with $I > 2\sigma(I)$	3686
indep reflns	801
indep reflns with $I > 2\sigma(I)$	630
R_{int} (obsd)	0.0176
Refinement	
refinement against	F^2
no. refined params	17
R/R_w[b] (obsd)	0.0176/0.0472
R/R_w (all)	0.0304/0.0528
GOF	0.93
residual electronic density ($e^-/Å^3$)	[−1.61; 0.90]

(b) Atomic Positions and Isotropic Thermal Parameters ($Å^2$)

atom	Wyckoff	*x*	*y*	*z*	U_{eq}
Pd	4a	0	0	0	0.01336(6)
Se	8c	0.11125(4)	0.11799(3)	0.40573(3)	0.01198(6)

(c) Anisotropic Thermal Parameters[c] ($Å^2$)

U_{11}	U_{22}	U_{33}	U_{12}	U_{13}	U_{23}
0.00785(9)	0.00762(9)	0.02461(13)	0.00020(6)	0.00049(8)	-0.00013(8)
0.00961(9)	0.00883(9)	0.01751(11).	0.00053(6)	-0.00026(7)	-0.00001(8)

[a] Determined from a Rietveld analysis on powder. [b] $R = \sum||F_o| - |F_c||/\sum|F_o|$. $R_w = [\sum w_F^2(|F_o|^2 - |F_c|^2)^2/\sum w_F^2|F_o|^4]^{1/2}$ with $w_F^2 = 1/(\sigma^2(I) + (2 \times 0.016I^2)$. [c] $U_{eq} = {}^1/_3\sum_i\sum_j U^{ij}a_i^*a_j^*\mathbf{a}_i\mathbf{a}_j$. $U^{ij*} = \exp[-2\pi^2(h^2a^{*2}U_{11} + k^2b^{*2}U_{22} + l^2c^{*2}U_{33} + 2hka^*b^*U_{12} + 2hla^*c^*U_{13} + 2klb^*c^*U_{23})]$.

of 1.85 GeV, was collimated by two sets of 50 μm-wide tungsten carbide slits. Exposure times ranged between 10 and 60 min, long enough to collect diffraction data with reasonable peak counts. Lattice parameters were least-squares refined with the GSAS crystallographic package.[17] To avoid most of the fluorescence and escape peaks, we considered X-ray diffraction (XRD) spectra only in the energy region from 16 to 50 keV (Table 2). Figure 2 shows the energy dispersive spectra of $PdSe_2$ determined under various pressures, where the fluorescence peaks of palladium (Kα and Kβ) are indicated by stars.

The peak shape was modeled by a modified gaussian function allowing for stress broadening associated with high pressure. The peak cutoff was set to 0.01% of the peak maximum. The background was manually adjusted. Refinement data are reported in Table 3 for three different pressures. The experimental, the calculated, and the difference plots determined at 7.6 GPa are represented in Figure 3. Unfortunately, the energy dispersive method was complicated by the high background, poor resolution, and intensity modeling. This limited the quality of data analysis. In addition, the domain of the powder sample explored by X-ray diffraction is very small so that the intensities are not collected with reliable crystallite orientation statistics.[18] As a result, it prevented us from doing Rietveld refinement.[19] Each recorded spectra was refined using the Le Bail method[20] with the conven-

(17) Larson, A. C.; Von Dreele, R. B. *General Structure Analysis System (GSAS)*; Los Alamos National Laboratory Report; Los Alamos National Laboratory: Los Alamos, NM, 2000.

Table 2. Values (in keV) of the Fluorescence and Escape Peaks of Pd and Se[a]

	palladium	selenium
fluorescence peaks	2.63 (L_η)	1.4 (L_α)
	21.2 (K_α)	11.2 (K_α)
	23.8 (K_β)	12.4 (K_β)
escape peaks	11.3 (K_α)	none
	13.9 (K_β)	

[a] The nature of the peaks is indicated in parentheses.

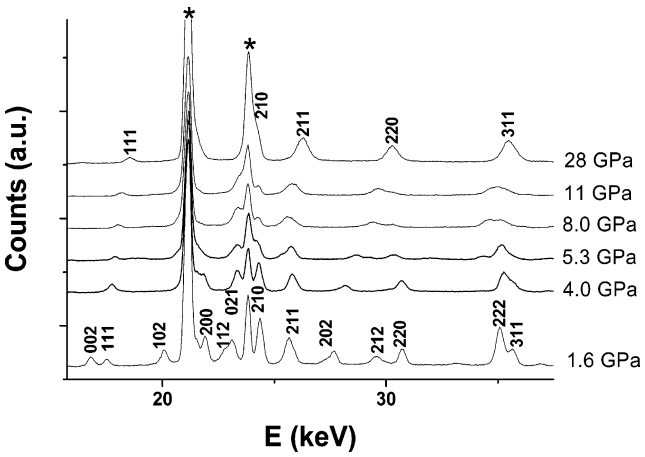

Figure 2. Energy dispersive spectra of $PdSe_2$ under various pressures. The asterisks (*) refer to the fluorescence peaks of palladium (Kα and Kβ lines). The peak positions refer to the PdS_2-type structure at 1.6 GPa, and to the pyrite-type structure at 28 GPa.

Table 3. Full Pattern Matching Refinement Data for $PdSe_2$ under Three Different Pressures[a]

	pressure (GPa)		
	2.4	7.6	28
exptl points	951	892	912
Rp	0.120	0.088	0.107
Rwp	0.157	0.123	0.136
reduced χ^2	7.5	3.9	9.0
refined params	8	14	6
structural type	PdS_2-type	PdS_2-type	pyrite-type	pyrite-type
a (Å)	5.738(2)	5.919(5)		
b (Å)	5.853(2)	5.867(5)	6.077(4)	5.902(1)
c (Å)	7.324(9)	6.518(18)		
A	$1.2(2) \times 10^{-4}$	$1.5(2) \times 10^{-3}$	$7.1(5) \times 10^{-4}$	
B	$-7.6(10) \times 10^{-3}$	$-9(1) \times 10^{-2}$	$-3.0(3) \times 10^{-3}$	
C	$1.5(2) \times 10^{-1}$	$1.4(1) \times 10^{-1}$	$3.3(3) \times 10^{-1}$	
ϵ_a	$-1.7(3) \times 10^{-3}$	$4(1) \times 10^{-3}$	$1.1(1) \times 10^{-2}$	$-1.6(5) \times 10^{-3}$
ϵ_A	$-1.6(6) \times 10^{-3}$	$-1.0(3) \times 10^{-2}$	$1.4(3) \times 10^{-2}$	$2.1(1) \times 10^{-3}$

[a] The gaussian broadening is given by a simple power series in energy: $\sigma = AE^2 + BE + C$. The energy dispersive spectra are affected by stress, so the reflection positions are given by a function of two coefficients ϵ_a and ϵ_A. $\Delta E = (E - E_{ph}) - \{\epsilon_a d \cos\theta + \epsilon_A [(hk)^2 + (hl)^2 + (kl)^2]/[h^2 + k^2 + l^2]\}E$.

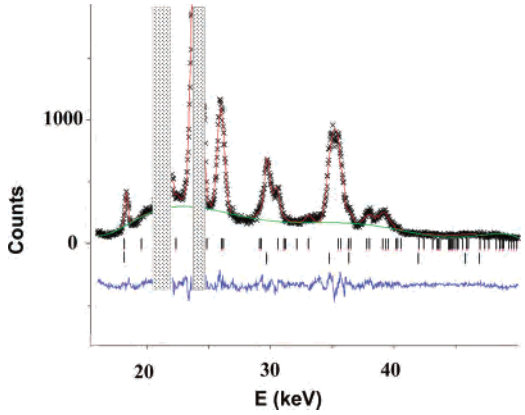

Figure 3. Experimental (×), calculated (—), and difference energy dispersive spectra of $PdSe_2$ under the pressure of 7.6 GPa. The shaded areas represent the excluded regions. The peak positions expected for the PdS_2-type structure are shown in the upper panel, and those for the pyrite-type structure are shown in the lower panel.

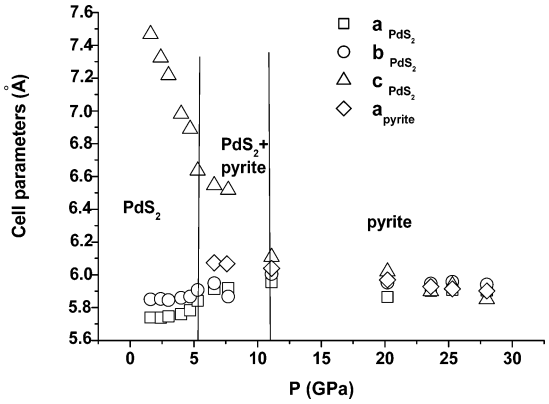

Figure 4. Cell parameters of $PdSe_2$ as a function of pressure.

tional *Pbca* and $Pa\bar{3}$ space groups for the PdS_2-type and the pyrite-type structures, respectively. In those refinements, the observed intensities in the narrow energy windows of 20.9−21.8 keV and 23.8−25.1 keV were excluded because they arise from the Pd fluorescence.

3. Structure Evolution of $PdSe_2$ under Pressure

3.1. Analysis of the XRD Patterns under Pressure. The pressure-dependence of the unit cell parameters was deduced in two ways. In the first step, each collected spectrum (from 1.6 to 30 GPa) was refined using the Le Bail method in the space group *Pbca*, i.e. under the assumption that only the PdS_2-type structure was present. At pressure higher than 6 GPa, two peaks (e.g., peaks at 30 and 35 keV at 6 GPa) could not be indexed with the considered space group and the selected unit cell. Their indexation requested the taking into account of a second phase with the pyrite structure type (see below). The results of these first-step refinements are summarized in Table 4a and Figure 4. As the pressure increases, the *c*-parameter sharply decreases while the *a*- and *b*-parameters slightly increase, and eventually, the three lattice parameters become similar at pressures above ca. 11 GPa (the parameters are not equal within the usual 3σ standard uncertainty because of the usual underestimation of the standard uncertainty in powder refinements). This indicates that only a cubic phase exists above 11 GPa. In view of the previous high pressure study[11] and the existing group to subgroup relation between the $Pa\bar{3}$ and *Pbca*, it is reasonable to assume that the cubic form has the pyrite-type structure. The transition is reversible as observed when the pressure is decreased with an hysteresis of about 5 GPa.

Table 4. Cell Parameters (Å) and Unit Cell Volume (Å^3) of $PdSe_2$ Determined as a Function of Pressure

(a) PdS_2-Type Structure Obtained from the First-Step Refinements (See Text)

P (GPa)	*a*	*b*	*c*	*V*
1.6	5.739(1)	5.850(1)	7.468(3)	250.7(2)
2.4	5.738(1)	5.853(2)	7.324(3)	246.0(2)
3.0	5.746(2)	5.846(2)	7.217(10)	242.4(5)
4.0	5.760(1)	5.859(2)	6.982(10)	235.6(5)
4.7	5.783(1)	5.867(2)	6.890(10)	233.8(5)
5.3	5.841(5)	5.907(5)	6.635(5)	228.9(6)
6.6	5.913(2)	5.949(3)	6.546(10)	230.3(5)
7.6	5.919(2)	5.867(2)	6.518(10)	226.3(5)
11.1	5.928(6)	6.005(8)	6.109(18)	218.5(12)
20.2	5.864(3)	5.952(4)	6.019(20)	210.1(9)
23.6	5.902(3)	5.946(3)	5.899(17)	207.0(8)
25.3	5.909(5)	5.958(4)	5.937(13)	209.0(8)
28.0	5.904(1)	5.941(3)	5.850(3)	205.2(2)

(b) PdS_2-Type Structure Obtained from the Second-Step Refinements (See Text)

P (GPa)	*a*	*b*	*c*	*V*
6.6	5.918(3)	5.934(4)	6.525(9)	229.1(6)
7.6	5.919(5)	5.867(5)	6.518(18)	226.3(10)
11.1	5.928(3)	5.972(5)	5.978(2)	211.6(4)

(c) Pyrite-Type Structure Obtained from the Second-Step Refinements (See Text)

P (GPa)	*a*	*V*
6.6	6.073(4)	224.0(3)
7.6	6.077(4)	223.4(3)
11.1	6.039(4)	220.2(3)
20.2	5.969(2)	212.7(3)
23.6	5.928(1)	208.3(1)
25.3	5.914(1)	206.8(1)
28.0	5.902(1)	205.6(1)

The cell parameter versus pressure plots show a clear discontinuity around 6 GPa (Figure 4). This observation, together with the fact that the two peaks (at 30 and 35 keV) occurring at pressure above 6 GPa cannot be indexed with the *Pbca* space group, indicates that both PdS_2- and pyrite-type structures coexist in the pressure region between 6 and 11 GPa. The two phases occur in the 6−11 GPa region probably because a slight pressure variation occurs in the diamond-anvil cell so that the pyrite-type structure forms in local areas where the pressure is greater than 11 GPa. Furthermore, the transformation of the PdS_2-type structure into a pyrite-type structure is expected to be of first order, so that the two phases should coexist for thermodynamic reasons. Thus, in the second step, the XRD patterns under pressure between 6 and 11 GPa were refined assuming the presence of both the PdS_2- and pyrite-type structures, while those under pressures higher than 12 GPa were refined assuming the presence of only the pyrite-type structure. The

(18) Paszkowicz, W. *Nucl. Instrum. Methods Phys. Res., Sect. B* **2002**, *198*, 142.
(19) Rietveld, H. M. *J. Appl. Crystallogr.* **1969**, *2*, 65.
(20) Le Bail, A.; Duroy, H.; Fourquet, J.-L. *Mater. Res. Bull.* **1988**, *23*, 447.

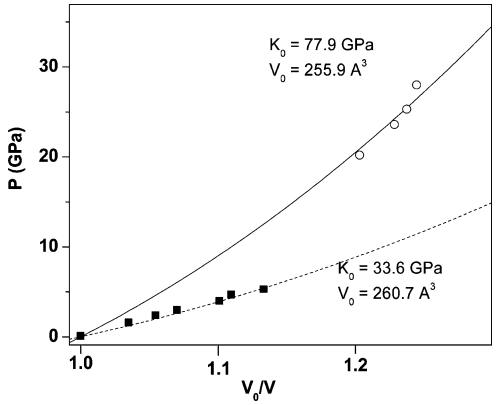

Figure 5. Variation of the relative volume for the PdS_2-type (■) and pyrite-type (○) structures of $PdSe_2$. The lines (— for PdS_2 and - - - for pyrite) represent equations of state with parameters given on the graph.

results of those second-step refinements are also summarized in Table 4b,c. The unit cell volumes of the PdS_2- and pyrite-type structures of $PdSe_2$ are estimated to differ by 2.9 Å^3 (i.e., 1.3% of the unit cell volume of the PdS_2-type structure) at 7.6 GPa where the two phases coexist. Under pressure above ca. 11 GPa, the three cell parameters determined for the PdS_2-type structure in the first-step refinements are practically the same as the cell parameter determined for the pyrite-type structure in the second-step refinements. Under pressure between 6 and 11 GPa, the three cell parameters determined for the PdS_2-type structure in the first-step refinements are practically the same as those in the second-step refinements.

The $P-V$ data of the orthorhombic and cubic phases were fitted to the second-order Birch−Murnaghan equation of state:[21] $P = 3/2K_0[(V_0/V)^{7/3} - (V_0/V)^{5/3}]$, where K_0 and V_0 are the bulk modulus and the cell volume at ambient pressure, and V is the volume at a given pressure. The fitting of the $P(V)$ curves lead to $K_0 = 33.6$ GPa and $V_0 = 260.7$ Å^3 (against $V_0 = 259.43$ (5) Å^3, see Table 1) for the orthorhombic form, and to $K_0 = 77.9$ GPa and $V_0 = 255.9$ Å^3 for the cubic form. As expected, due the great difference in the dimensionality of the two phases, the bulk modulus of the PdS_2 form is much smaller compared with that of the pyrite form, while the cell volume V_0 is contracted from the low pressure form to the high pressure form ($\Delta V_0 = 4.8$ Å^3, ca. 1.2 Å^3 per formula unit). The pressure dependence of the relative volumes V_0/V of the PdS_2- and pyrite-type structures is presented in Figure 5.

Thus, the structural transition of $PdSe_2$ under pressure is essentially described as a contraction of the gap along the c-axis length of the PdS_2-type structure, which decreases the two long interlayer Pd···Se distances around each Pd to form six equivalent Pd−Se bonds. Due to the nonisomorphic subgroup−supergroup relation between the PdS_2-type (*Pbca*) and the pyrite-type ($Pa\bar{3}$) structures, the nature of the phase transition is displacive.[22]

3.2. First Principles Electronic Band Structure Analysis. Calculations. The $PdSe_2$ lattice parameters and atomic positions were optimized at a given external, isotropic pressure or at a constant cell volume by means of electronic band structure calculations using the Vienna ab initio simulation package (VASP),[23−25] on the basis of the local-density approximation. Our calculations used ultra soft pseudo-potentials, constructed using the Vanderbilt recipe,[26,27] and a conjugate gradient scheme to relax the ions into their instantaneous ground state. The integration in the Brillouin zone was performed on a set of 48 special k points determined by the Monckhorst−Pack scheme. All calculations were carried out using the generalized gradient approximation, as described by Perdew and Wang.[28]

Pressure Study. Using a specified external pressure, we examined, after relaxation, the space group (by means of the Endeavor package[29]), cell volume, atomic positions, and total energy as a function of pressure. At 0 GPa, the PdS_2-type structure is well reproduced by calculations in the *Pbca* space group (e.g., the unit cell parameters optimized by VASP calculations are $a = 5.875$ Å, $b = 5.982$ Å and $c = 7.772$ Å, which are in satisfactory agreement with experiment). Similar results are obtained from our calculations performed for ambient pressure. For pressures higher than 1 GPa, however, calculations predict that $PdSe_2$ adopts the pyrite-type structure rather than the PdS_2-type structure, in disagreement with our experimental observation that $PdSe_2$ adopts the pyrite-type structure at pressure near 11 GPa. The discrepancy between the experimental and calculated values may originate most likely from the inaccuracy inherent in the calculations. For the $PdSe_2$ system, VASP calculations are unreliable when both the unit cell volume and the atom positions are optimized simultaneously under a given pressure. Therefore, we optimized only the atom positions and the cell parameters to determine whether the PdS_2- or pyrite-type structure is more stable at a given unit cell volume. We carried out these calculations as a function of the unit cell volume because decreasing the cell volume is equivalent to increasing the applied pressure. Again, at the final step of the refinement process, the symmetry of the unit cell was carefully examined.

The total energy of $PdSe_2$ as a function of the cell volume is summarized in Figure 6a, where the structure type adopted at a given volume is also indicated. The preferred structure is the PdS_2-type structure when the cell volume is greater than ∼250 Å^3 (against ∼225 Å^3 experimentally), but the pyrite-type structure when the volume is reduced below ∼250 Å^3. The total energy is nearly constant when the cell volume is greater than ∼250 Å^3, and it increases steadily as the cell volume is reduced. Thus, the plot of the energy versus the cell volume shows that the pyrite structure can be adopted only when the cell volume is reduced enough, i.e., when the

(21) Birch, F. *Phys. Rev.* **1947**, *71*, 809.
(22) Winkler, B.; Pickard, C. J.; Segall, M. D.; Milman, V. *Phys. Rev. B* **2001**, *63*, 214103.
(23) Kresse G.; Furthmüller, J. *Vienna Ab initio Simulation Package (VASP)*; Institut für Materialphysik, Universität Wien: Austria. See also: http://cms.mpi.univie.ac.at/VASP/.
(24) Kresse G.; Furthmüller, J. *Comput. Sci.* **1996**, *6*, 15.
(25) Kresse G.; Furthmüller, J. *Phys. Rev. B* **1996**, *54*, 11169.
(26) Vanderbilt, D. *Phys. Rev. B* **1991**, *41*, 7892.
(27) Kresse G.; Furthmüller, J. *J. Phys.: Condens. Matter* **1994**, *6*, 8245.
(28) Perdew J. P.; Wang, Y. *Phys. Rev B* **1996**, *33*, 8800.
(29) Putz, H.; Schoen, J. C.; Jansen, M. *J. Appl. Crystallogr.* **1999**, *32*, 864.

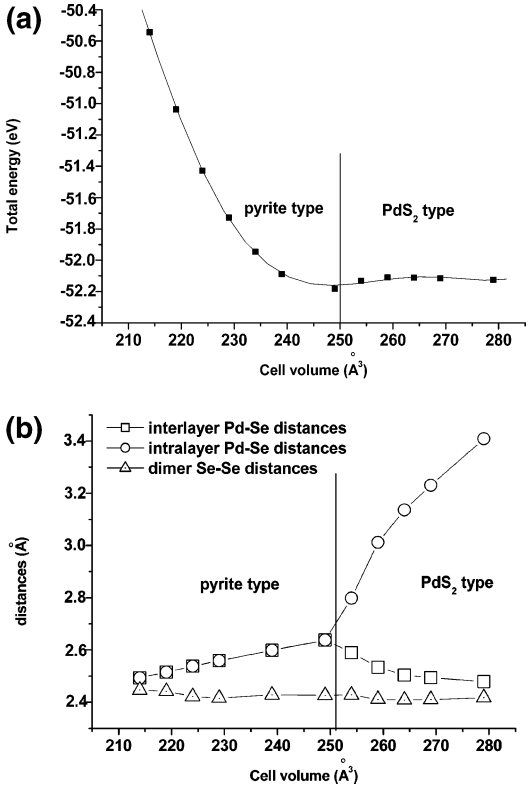

Figure 6. (a) Total energy and preferred structure of $PdSe_2$ calculated as a function of the unit cell volume. (b) Variation of the intralayer and interlayer Pd−Se distances of the PdS_2-type structure, the Pd−Se distance of the pyrite-type structure, and the dimer Se−Se distances of the PdS_2-type and pyrite-type structures calculated as a function of the unit cell volume.

external pressure is strong enough. Figure 6b plots, as a function of the unit cell volume, the intra- and interlayer Pd−Se bond distances of the PdS_2-type structure, the Pd−Se distance of the pyrite-type structure, and the intradimer Se−Se bond distances of the PdS_2- and pyrite-type structures. Clearly, as the unit cell volume of the PdS_2-type structure is decreased, the long interlayer Pd−Se distance is sharply reduced while the intralayer Pd−Se distance is slightly increased. As the unit cell volume of the pyrite-type structure is decreased, the Pd−Se distance is steadily reduced. In contrast, the intradimer Se−Se bond distance remains nearly constant throughout the unit cell volume decrease. These observations are entirely consistent with the experimental conclusion that all parameter changes at the structural transition of $PdSe_2$ under pressure essentially involve a contraction of the *c*-axis length, thereby decreasing the two long interlayer Pd···Se distances around each Pd to form six equivalent Pd−Se bonds.

4. Electronic Factors Affecting the Structural Preference of MQ_2 (M = Ni, Pd, Pt)

It is of interest to probe why $PdSe_2$ under ambient pressure adopts the PdS_2-type structure, but not the pyrite-type structure. For this purpose, it is convenient to examine the PdS_2- and pyrite-type structures of MSe_2 (M = Pd, Ni) from the viewpoint of stacking the puckered MSe_2 layers under the assumption that the structure of each puckered MSe_2 layers remains constant. Then, the structure of $PdSe_2$ becomes the pyrite-type structure; i.e., the intralayer and interlayer Pd−Se distances become nearly equal, when the interlayer spacing is reduced by approximately 1.0 Å. The structure of $NiSe_2$ becomes the PdS_2-type structure, i.e., the ratio of the intralayer Ni−Se to the interlayer Ni−Se distances becomes close to 0.69 as found for the PdS_2-structure of $PdSe_2$, when the interlayer spacing is increased by approximately 1.25 Å.

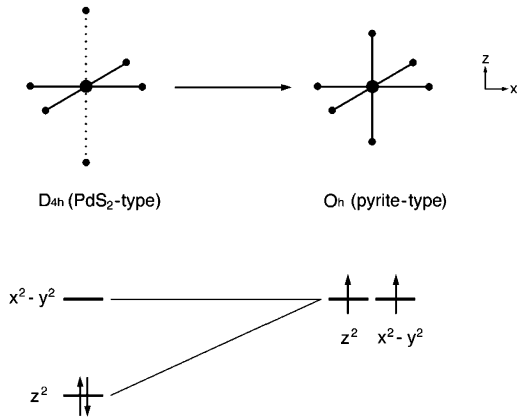

Figure 7. Schematic orbital correlation diagram for the two highest d-block levels of a local PdQ_6 polyhedron (Q = S, Se) between the PdS_2- and pyrite-type structures.

As depicted in Figure 7 the local electronic structure of a $PdSe_6$ polyhedron in $PdSe_2$ can be represented by the low-spin configuration $(z^2)^2(x^2 - y^2)^0$ in the PdS_2-type structure (D_{4h} $PdSe_6$), but by the high-spin configuration $(z^2)^1(x^2 - y^2)^1$ in the pyrite-type structure (O_h $PdSe_6$). In a sense, the structural change of $PdSe_2$ from the pyrite-type to the PdS_2-type structure can be regarded as a "Jahn−Teller" distortion of each $PdSe_6$ octahedron. Our EHTB calculations[30,31] show that $PdSe_2$ becomes steadily less stable as the interlayer spacing is reduced toward the pyrite-structure, with the pyrite-type structure being less stable than the PdS_2-type structure by ∼5 eV per formula unit (from first principles calculations, the stability of the two $PdSe_2$ forms are very similar, i.e., less than 19 meV/unit formulas different). This result is consistent with experiment, and supports the view that the structural change from the pyrite-type to the PdS_2-type structure can be considered as a "cooperative Jahn−Teller" distortion.[32]

The primary cause for the PdS_2-structure of $PdSe_2$ is the interlayer overlap repulsion that arises from the overlap of the filled $4d_z^2$ orbitals of the Pd in one $PdSe_2$ layer with the filled π^* orbitals of the $(Se_2)^{2-}$ anions in the adjacent $PdSe_2$ layers. This interlayer overlap repulsion effect should also be present in $NiSe_2$. However, the $3d_z^2$ orbital of Ni has a smaller spatial extension than does the $4d_z^2$ orbital of Pd, so that the interlayer overlap repulsion should be weaker in

(30) Whangbo, M.-H.; Hoffman, R. *J. Am. Chem. Soc.* **1978**, *100*, 6397.
(31) Our calculations were carried out employing the CAESAR program package. (Ren, J.; Liang, W.; Whangbo, M.-H. *Crystal And Electronic Structure Analysis Using CAESAR*; 1998. Free download from http://chvamw.chem.ncsu.edu/.)
(32) (a) Kugel, K. I.; Khomskii, D. I. *Sov. Phys. Usp.* **1982**, *25*, 231. (b) Whangbo, M.-H.; Koo, H.-J. *Solid State Sci.* **2002**, *4*, 335.

$NiSe_2$ than in $PdSe_2$. This expectation is borne out by our EHTB calculations for $NiSe_2$, which predict that the pyrite-type structure is less stable than the PdS_2-type structure by ~2.5 eV per formula unit, half the corresponding difference in $PdSe_2$ (from DFT calculations, any attempt to optimize the geometry of an hypothetical PdS_2 form of $NiSe_2$ yielded the experimentally observed, pyrite structure).

Our EHTB calculations for $NiSe_2$ led to an incorrect prediction that the PdS_2-type structure is more stable than the pyrite-type structure. It is important to consider what energy factors, not well represented in EHTB calculations, favor the pyrite-type structure over the PdS_2-type structure in $NiSe_2$. The Ni−Se bond is expected to be more ionic than the Pd−Se bond, which makes $NiSe_2$ more ionic than $PdSe_2$. Thus, the Ni^{2+} ions prefer to have octahedral, six-coordinate environments than square planar, four-coordinate environments. In addition, the Ni 3d orbitals are more contracted than are the Pd 4d orbitals. Consequently, the on-site repulsion U in the doubly occupied d_z^2 orbital of the PdS_2-type structure is greater in $NiSe_2$ than in $PdSe_2$. Therefore, it is suggested that $NiSe_2$ adopts the pyrite-type structure because the effect of the ionic interaction and the on-site repulsion dominates over that of the interlayer overlap repulsion, but that $PdSe_2$ adopts the PdS_2-type structure because the opposite is true.

On the basis of the above reasoning, the PdS_2-type structure would be favored over the pyrite-type structure for $PtSe_2$. As already mentioned, $PtSe_2$ adopts the CdI_2-type structure[10,33] in which the Se atoms exist as isolated anions instead of dimer anions $(Se_2)^{2-}$. Each transition metal of dichalcogenide MQ_2 has six M−Q bonds in the CdI_2-type structure, but four M−Q bonds and one Q−Q bond in the PdS_2-type structure. Therefore, the CdI_2-type structure should be favored over the PdS_2-type structure if the covalent character of the M−Q bond becomes stronger. The Pt−Se bond should be more covalent than the Pd−Se bond, because the Pt 5d orbital should overlap better with the Se 4p orbital than does the Pd 4d orbital. This explains why $PtSe_2$ adopts the CdI_2-type structure rather than the PdS_2-type structure.

5. Concluding Remarks

Our pressure-dependent X-ray diffraction measurements of $PdSe_2$ at room temperature show that $PdSe_2$ undergoes a reversible phase transition from the PdS_2-type to the pyrite-type structure around 10 GPa. In essence, the applied pressure reduces the spacing between adjacent $^2/_\infty[PdSe_2]$ layers of the PdS_2-type structure to form the three-dimensional lattice of the pyrite-type structure. The pressure-dependent structural change of $PdSe_2$ is well reproduced by first principles electronic band structure calculations carried out for $PdSe_2$ as a function of the unit cell volume. This study indicates that these calculations can be used to investigate and predict the behavior of compounds under pressure. Analysis of the relative stability of the pyrite-type and the PdS_2-type structures using extended Hückel calculations suggests that the structural change from the pyrite-type to the PdS_2-type structure can be regarded as a "cooperative Jahn−Teller" distortion, and the primary cause for the PdS_2-type structure of $PdSe_2$ is the interlayer overlap repulsion. It is suggested that $NiSe_2$ adopts the pyrite-type structure because the Ni/Se ionic interaction and the on-site repulsion of the Ni d_z^2 orbital dominates over the interlayer overlap repulsion, and that $PtSe_2$ adopts the CdI_2-type structure because the Pt−Se bond is more strongly covalent than the Pd−Se bond.

Acknowledgment. Work at North Carolina State University was supported by the Office of Basic Energy Sciences, Division of Materials Sciences, U.S. Department of Energy, under Grant DE-FG02-86ER45259. We also acknowledge the LURE for beam time allocation (Proposal DH 301-02).

Supporting Information Available: X-ray crystallographic file in CIF format for the structure determination of $PdSe_2$ in ambient conditions. This material is available free of charge via the Internet at http://pubs.acs.org.

IC0352396

(33) Furuseth, S.; Selte, K.; Kjekshus, A. *Acta Chem. Scand.* **1988**, *1*, 1973.